

cluding the redox state of the intracellular nicotinamide adenine dinucleotide [NAD(H)] pool (27). Any number of these effects may contribute, both directly and indirectly, to the ultimate architectures observed. One component that is likely involved is extracellular polysaccharide (EPS). Congo Red, a constituent of the agar used in the experiments shown in Fig. 3, is known to bind the glucose-rich exopolysaccharide PEL (28). Because the phenazine-null mutant is bright red, whereas the pyocyanin overproducer is pale, we infer there is an inverse relationship between phenazine and PEL production (Fig. 3). How phenazines affect the *pel* genes and how such changes in EPS composition contribute to colony morphogenesis remain to be determined.

Pigments excreted by bacteria have long been assumed to be “secondary” metabolites or even waste products, owing to the sporadic strain- and condition-dependent nature of their production (29). Many of these redox-active compounds are known to have antibiotic activities toward competing cells (1, 20), but until recently, their potential to directly participate in the physiology of the producing organism has been largely neglected (7). We now know that small molecules initially characterized as antibiotics allow intercellular communication within bacterial populations (30), and this work implies a conserved function for redox-active pigment antibiotics of the Gram-negative bacterium *P. aeruginosa* and the Gram-positive bacterium *S. coelicolor* A3(2). These pigments influence transcriptional regulation and modulate the phys-

ical characteristics of communities of their producers at later stages in their development. Rather than being “secondary,” diverse redox-active antibiotics may share similar functions of primary importance throughout the bacterial domain.

#### References and Notes

- D. V. Mavrodi, W. Blankenfeldt, L. S. Thomashow, *Annu. Rev. Phytopathol.* **44**, 417 (2006).
- A. Price-Whelan, L. E. Dietrich, D. K. Newman, *Nat. Chem. Biol.* **2**, 71 (2006).
- S. Mahajan-Miklos, M. W. Tan, L. G. Rahme, F. M. Ausubel, *Cell* **96**, 47 (1999).
- M. Mazzola, R. J. Cook, L. S. Thomashow, D. M. Weller, L. S. Pierson 3rd, *Appl. Environ. Microbiol.* **58**, 2616 (1992).
- M. E. Hernandez, A. Kappler, D. K. Newman, *Appl. Environ. Microbiol.* **70**, 921 (2004).
- Y. Wang, D. K. Newman, *Environ. Sci. Technol.* **42**, 2380 (2008).
- M. E. Hernandez, D. K. Newman, *Cell. Mol. Life Sci.* **58**, 1562 (2001).
- L. E. Dietrich, A. Price-Whelan, A. Petersen, M. Whiteley, D. K. Newman, *Mol. Microbiol.* **61**, 1308 (2006).
- S. I. Liochev, L. Benov, D. Touati, I. Fridovich, *J. Biol. Chem.* **274**, 9479 (1999).
- P. J. Pomposiello, B. Dimple, *J. Bacteriol.* **182**, 23 (2000).
- I. R. Tsaneva, B. Weiss, *J. Bacteriol.* **172**, 4197 (1990).
- W. Park, S. Pena-Llopis, Y. Lee, B. Dimple, *Biochem. Biophys. Res. Commun.* **341**, 51 (2006).
- K. Kobayashi, S. Tagawa, *J. Biochem.* **136**, 607 (2004).
- M. Palma *et al.*, *Infect. Immun.* **73**, 2958 (2005).
- Materials and methods are available as supporting material on Science Online.
- W. Eiamphungporn, N. Charoenlap, P. Vattanaviboon, S. Mongkolsuk, *J. Bacteriol.* **188**, 8669 (2006).
- E. Cundliffe, *Annu. Rev. Microbiol.* **43**, 207 (1989).
- J. M. Turner, A. J. Messenger, *Adv. Microb. Physiol.* **27**, 211 (1986).

- D. A. Hopwood, *Streptomyces in Nature and Medicine: The Antibiotic Makers* (Oxford Univ. Press, Oxford, 2007).
- K. F. Chater, *Philos. Trans. R. Soc. Lond. B Biol. Sci.* **361**, 761 (2006).
- B. Floriano, M. Bibb, *Mol. Microbiol.* **21**, 385 (1996).
- D. G. Davies *et al.*, *Science* **280**, 295 (1998).
- V. S. Maddula, Z. Zhang, E. A. Pierson, L. S. Pierson 3rd, *Microb. Ecol.* **52**, 289 (2006).
- K. Tahlan *et al.*, *Mol. Microbiol.* **63**, 951 (2007).
- S. Aendeker *et al.*, *Microbiology* **151**, 1113 (2005).
- X. Z. Li, N. Barre, K. Poole, *J. Antimicrob. Chemother.* **46**, 885 (2000).
- A. Price-Whelan, L. E. Dietrich, D. K. Newman, *J. Bacteriol.* **189**, 6372 (2007).
- L. Friedman, R. Kolter, *Mol. Microbiol.* **51**, 675 (2004).
- R. P. Williams, *Bacteriol. Rev.* **20**, 282 (1956).
- G. Yim, H. H. Wang, J. Davies, *Philos. Trans. R. Soc. London B Biol. Sci.* **362**, 1195 (2007).
- Single-letter abbreviations for the amino acid residues are as follows: A, Ala; C, Cys; D, Asp; E, Glu; F, Phe; G, Gly; H, His; I, Ile; K, Lys; L, Leu; M, Met; N, Asn; P, Pro; Q, Gln; R, Arg; S, Ser; T, Thr; V, Val; W, Trp; Y, Tyr; and X, any amino acid.
- S. Mehra *et al.*, *J. Ind. Microbiol. Biotechnol.* **33**, 159 (2006).
- We thank P. Straight (Harvard University); M. Bibb and A. Hesketh (John Innes Centre, UK) for providing *S. coelicolor* A3(2) strains M145 and M512; and N. C. Caiazza, C. T. Brown, and B. Wold for helpful discussions. This work was supported by an EMBO Long Term Fellowship (L.E.P.D.) and grants from the Packard Foundation and Howard Hughes Medical Institute (D.K.N.).

#### Supporting Online Material

www.sciencemag.org/cgi/content/full/321/5893/1203/DC1  
Materials and Methods  
Figures S1 to S5  
Table S1  
References

19 May 2008; accepted 24 July 2008  
10.1126/science.1160619

## Solution Structure of the Integral Human Membrane Protein VDAC-1 in Detergent Micelles

Sebastian Hiller,<sup>1</sup> Robert G. Garces,<sup>1\*</sup> Thomas J. Malia,<sup>1\*†</sup> Vladislav Y. Orekhov,<sup>1,3</sup> Marco Colombini,<sup>2</sup> Gerhard Wagner<sup>1,3‡</sup>

The voltage-dependent anion channel (VDAC) mediates trafficking of small molecules and ions across the eukaryotic outer mitochondrial membrane. VDAC also interacts with antiapoptotic proteins from the Bcl-2 family, and this interaction inhibits release of apoptogenic proteins from the mitochondrion. We present the nuclear magnetic resonance (NMR) solution structure of recombinant human VDAC-1 reconstituted in detergent micelles. It forms a 19-stranded  $\beta$  barrel with the first and last strand parallel. The hydrophobic outside perimeter of the barrel is covered by detergent molecules in a beltlike fashion. In the presence of cholesterol, recombinant VDAC-1 can form voltage-gated channels in phospholipid bilayers similar to those of the native protein. NMR measurements revealed the binding sites of VDAC-1 for the Bcl-2 protein Bcl-x<sub>L</sub>, for reduced  $\beta$ -nicotinamide adenine dinucleotide, and for cholesterol. Bcl-x<sub>L</sub> interacts with the VDAC barrel laterally at strands 17 and 18.

The integral membrane protein VDAC forms the primary path for diffusion of metabolites between the mitochondrial intermembrane space and the cytosol (1, 2). VDAC is conserved across eukaryotes, with about 30% sequence identity between yeast and human. The three isoforms, VDAC-1, VDAC-2, and VDAC-3,

found in humans are 68% to 75% pairwise identical. All three isoforms allow the exchange of metabolites through the membrane but have distinct physiological roles and expression profiles (3, 4).

Numerous reports have suggested that VDAC-1 is involved in mitochondrial apoptosis (5–7).

Apoptotic signals lead to the formation of a mitochondrial exit channel that allows the release of apoptogenic proteins, which in turn cause cell death by activating executioner caspase or through other mechanisms (8–10). Functional studies indicate that VDAC-1 closure leads to the opening of the mitochondrial exit channel (11). The anti-apoptotic protein Bcl-x<sub>L</sub> opens the VDAC-1 channel for trafficking of metabolites and thus inhibits the release of apoptogenic proteins (12). Direct interaction between VDAC-1 and Bcl-x<sub>L</sub> has been demonstrated (11, 13).

Insights into VDAC organization have come from biochemical and biophysical studies (14, 15) and low-resolution electron microscopy (EM) data showing that VDAC-1 is a cylindrical channel with a diameter of 20 to 30 Å (16, 17). Electrophysiological experiments revealed that, at low membrane potentials of 10 mV, VDAC is in the open state, but it switches to the closed state at

<sup>1</sup>Department of Biological Chemistry and Molecular Pharmacology, Harvard Medical School, Boston, MA 02115, USA.

<sup>2</sup>Department of Biology, University of Maryland, College Park, MD 20742, USA. <sup>3</sup>Swedish NMR Centre, University of Gothenburg, Box 465, 40530 Gothenburg, Sweden.

\*These authors contributed equally to this work.

†Present address: Centocor, Incorporated, Radnor, PA 19087, USA.

‡To whom correspondence should be addressed. E-mail: gerhard\_wagner@hms.harvard.edu

increased membrane potentials of about 30 mV (18). Thus, Donnan or diffusion potentials across the outer mitochondrial membrane may regulate small-molecule passage (19). In a lipid bilayer, recombinant VDAC can form stable open states and feature voltage-dependent transitions (20).

We present the three-dimensional (3D) solution structure of human VDAC-1 reconstituted in detergent micelles as determined by high-resolution nuclear magnetic resonance (NMR). We have assayed the binding of VDAC-1 with two natural ligands, reduced  $\beta$ -nicotinamide adenine dinucleotide ( $\beta$ -NADH) and cholesterol, and with the protein Bcl-x<sub>L</sub> by NMR and identified the location of these interaction sites on the structure of VDAC-1.

For the structure determination of VDAC-1 with NMR spectroscopy, we refolded bacterially expressed human VDAC-1 into lauryldimethylamine oxide (LDAO) detergent micelles (21). The channel exhibits a well-dispersed 2D [<sup>15</sup>N, <sup>1</sup>H]-TROSY (transverse relaxation optimized spectroscopy) spectrum indicating the presence of extensive  $\beta$  sheet secondary structure (fig. S1). High-field triple-

resonance TROSY-type experiments and selective labeling enabled sequence-specific resonance assignment of 80% of the protein backbone, including the C <sup>$\beta$</sup>  resonances (Fig. 1 and figs. S2 and S3). Nineteen  $\beta$  strands are formed within residues 25 to 283, and a short  $\alpha$  helix is located at the N terminus containing residues 6 to 10, as indicated by C <sup>$\alpha$</sup>  and C <sup>$\beta$</sup>  secondary chemical shifts (fig. S4). To complement the backbone assignments, we prepared specifically isotope-labeled samples to assign methyl groups of Ile, Leu, and Val residues (22) (fig. S5). These side-chain assignments were essential for defining the overall structure of the protein and the location of the N-terminal helix with respect to the channel.

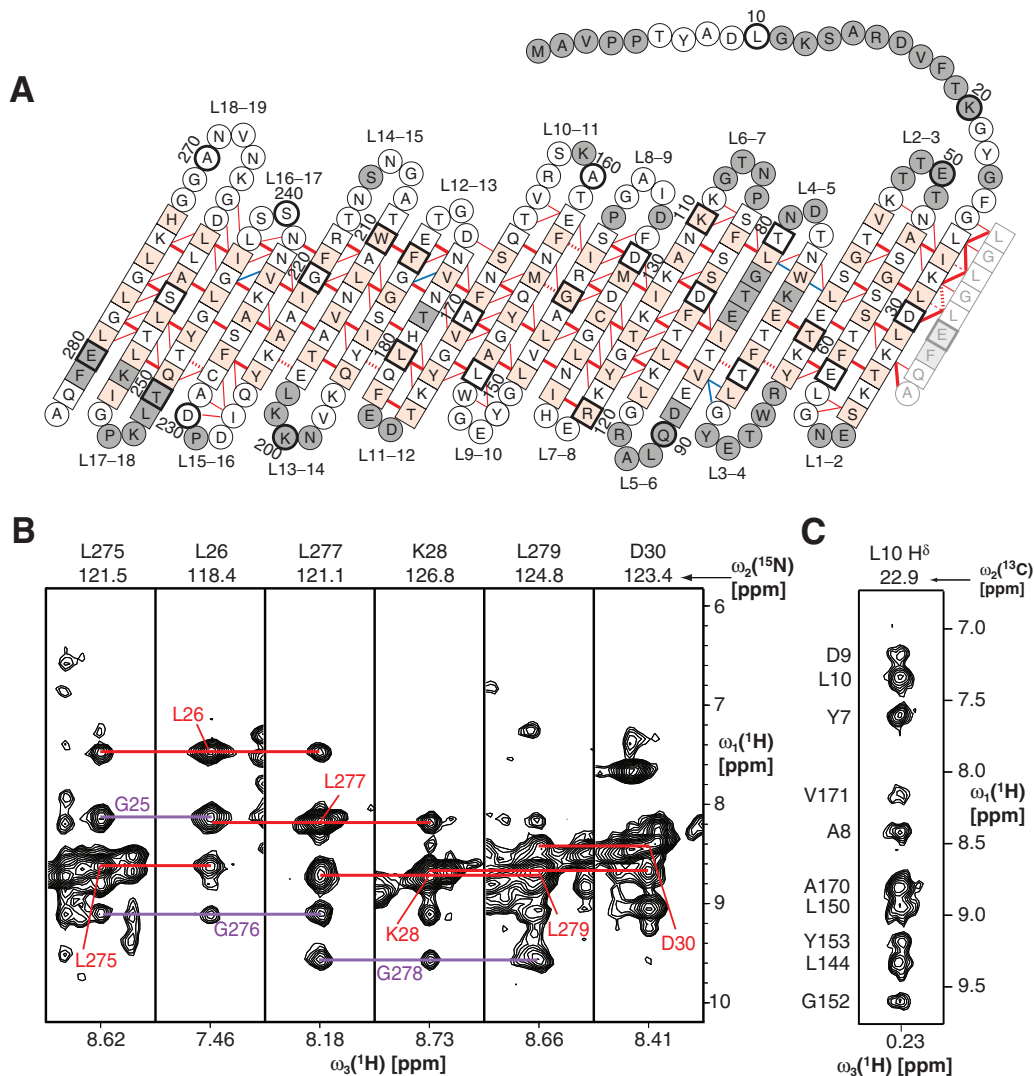
For the acquisition of long-range structural information, we used nuclear Overhauser effect spectroscopy (NOESY) to establish spatial correlations between nuclear spins (23). To obtain adequate signal, we needed to record these NOESY experiments on a fully deuterated background, including the use of perdeuterated LDAO molecules. From the cross-peaks observed in 3D and

4D NOESY experiments, we identified a network of more than 600 NOE contacts that confirmed the 19-stranded  $\beta$  sheet topology for VDAC-1 in LDAO micelles and established the relative orientation of the strands (Fig. 1, figs. S6 and S7, and table S1). Strands 1 to 19 form an antiparallel  $\beta$  sheet, which is closed to a  $\beta$  barrel by parallel pairing of strands 19 and 1.

Thirty-two discrete  $\beta$ -barrel membrane protein structures have so far been solved, all from prokaryotic organisms and all consisting of even numbers of  $\beta$  strands with antiparallel orientation (24) (fig. S8). The eukaryotic VDAC-1 thus represents a new class of a  $\beta$ -barrel membrane protein fold. Whereas N- and C-terminal ends are aligned next to each other in even-stranded barrels, they protrude from opposite sides of the VDAC-1 barrel. However, the N terminus of VDAC reaches through the channel to return to the same side of the barrel as the C terminus. In previous predictions of the VDAC topology, the number of  $\beta$  strands ranged from 12 to 19, with one corresponding to the topology determined here (25).

### Fig. 1. Architecture of VDAC-1. (A)

The amino acid sequence of VDAC-1 in one-letter code (36) is arranged according to the secondary and tertiary structure. Amino acids in squares denote  $\beta$  sheet secondary structure as identified by secondary chemical shifts; all other amino acids are in circles. Red and blue lines denote experimentally observed NOE contacts between two amide protons and NOE contacts involving side chain atoms, respectively. Bold lines indicate strong NOEs typically observed between hydrogen-bonded residues in  $\beta$  sheets. For clarity of the presentation, not all observed NOEs are shown. The 19th strand is duplicated at the right, next to strand 1, to allow for indicating the barrel-closure NOEs. The side chains of white and orange residues point toward the inside and the outside of the barrel, respectively. Dashed lines show probable contacts between protons with degenerate <sup>1</sup>H chemical shifts. Gray residues could not be assigned so far. Every 10th amino acid is marked with a heavy outline, and corresponding residue numbers are indicated. (B) Strips from a 3D [<sup>1</sup>H, <sup>1</sup>H]-NOESY-<sup>15</sup>N-TROSY defining the barrel closure between parallel strands 1 and 19. Red lines show the interstrand contacts for the depicted residues, whereas the violet lines indicate the NOE contacts for the respective opposite residues. ppm, parts per million. (C) Strip from a 3D [<sup>1</sup>H, <sup>1</sup>H]-NOESY-<sup>13</sup>C-HMQC (heteronuclear multiple-quantum coherence) taken at the position of a methyl group of Leu<sup>10</sup>. The assignments of the individual NOE signals are indicated on the left and exemplify the NOEs defining the location of the N-terminal helix in the barrel. The frequency axes  $\omega_1$ ,  $\omega_2$ , and  $\omega_3$  are indicated.



On the basis of the experimental constraints, we calculated the 3D structure for VDAC-1 in LDAO micelles (Fig. 2 and table S1). The 19  $\beta$  strands form the wall of an open barrel with the strands being tilted by about  $45^\circ$  with respect to the barrel main axis. Alternating between the two ends of the barrel, adjacent strands are connected by loops with lengths of 2 to 10 residues. The height of the barrel including the loops is about 30 Å, and a circular conformer of VDAC-1 has an open diameter of about 25 Å, corresponding nicely to EM data (16, 17).

Consistent with the function of VDAC-1 as a wide diffusion pore, no tertiary contacts were observed between residues across the barrel diameter. This is reflected within the calculated bundle of 20 structural conformers, among which the  $\beta$  barrel adopts differently circular and oval shapes (fig. S9). It is unclear whether this variation of the barrel shape represents actual molecular motions. The relative orientations of the  $\beta$  strands with respect to each other are well defined by the observed NOEs and thus identical in all members of the conformational ensemble.

The N-terminal tail of VDAC-1, consisting of residues 1 to 23, is not part of the barrel wall but is located inside the channel. NOE contacts connect residues 7, 8, 9, and 10 with several residues around a small hydrophobic patch formed by residues Val<sup>143</sup> (V143) and Leu<sup>150</sup> (L150) on the inside of the barrel wall (Figs. 1 and 2). The observation that the N-terminal 23 residues are structurally not involved in the main barrel architecture is consistent with experiments showing that a deletion mutant with the N-terminal part missing properly targets to the mitochondrial outer membrane (26). Because the N-terminal region is involved in voltage gating (27), this segment might adopt different conformations depending on the external conditions.

The overall theoretical charge of VDAC-1 at neutral pH is +3, because 29 negative charges from Asp and Glu residues oppose 32 positive charges from Arg and Lys residues. These charges are located predominantly in the loops and in the interior, water-accessible wall of the channel, where they cluster to form one negative and two positive patches (Fig. 2). The VDAC channel is known to be open to both anions and cations, with a 2:1 preference for anions (28, 29); thus, these two features of the channel could be correlated.

The surface of VDAC-1 that is in contact with the detergent micelle was determined with the help of the detergent 16-doxyl stearic acid (16-DSA), which has a paramagnetic spin label attached to its hydrophobic tip, quenching all NMR resonances of residues in close contact with the micelle interior (30). The data show that the detergent micelle covers the entire periphery of the VDAC-1 barrel like a belt, corresponding to the position of hydrophobic residues on the outside of the barrel (Fig. 3 and fig. S10). On the inner wall, only two hydrophobic residues are located, the above-mentioned L150 and V143 (Fig. 3C). Thus, the protein-micelle complex in aqueous

solution has a topology that would be consistent with the assumption that the protein adopts a similar fold in a lipid bilayer as in the LDAO micelle. The data obtained in the micellar state cannot address which opening of the channel faces into the mitochondria and which faces into the cytosol. Previous studies attempting to determine this orientation have reached different conclusions (15, 31). Experiments on *Neurospora crassa* VDAC suggested a different barrel topology and proposed a membrane-inserted N-terminal helix (32), which is inconsistent with the structure presented here. The VDAC-1 solution structure will stimulate revisiting the large body of previous biochemical data and the design of new experiments to resolve this issue.

The possibility of a multimeric state of VDAC is a matter of ongoing debate. There is evidence to support the formation of dimers, trimers, and tetramers, possibly in dynamic equilibrium with monomers (13). Because the entire perimeter of VDAC-1 is in contact with the micelle-immersed spin labels (Fig. 3A), our data exclude formation of stable oligomers in the LDAO micelles; however, a dynamic interchannel interaction cannot be excluded. A possible interaction site is located on strands 4 and 5, where the resonances of several residues are unresolved presumably because of exchange broadening (Fig. 1). This potential contact may be due to the high protein/detergent

ratio used here and may not exist in mitochondrial membranes.

In its native environment in the outer mitochondrial membrane, VDAC has several post-translational modifications such as phosphorylation and acetylation (33). In an attempt to determine whether these affect function, we compared the gating parameters of our unmodified recombinant protein with those of native VDAC carrying post-translational modifications. To achieve functional properties similar to wild-type, recombinant VDAC-1 had to be reconstituted into planar membranes in the presence of cholesterol and the detergent triton X100, which were both also present in the reference measurements with native VDAC (34, 35). Under these conditions, the refolded VDAC-1 exhibited functional behavior similar to that of native VDAC from eukaryotic sources as measured by the single-channel conductance, the effective valence of the voltage sensor, the energy difference between open and closed states ( $\Delta E_{\text{open/closed}}$ ), and ion selectivity (fig. S11 and Table 1). Although the present data do not directly address the structure of VDAC-1 in lipid bilayers, it is clear that our recombinantly produced VDAC-1 polypeptide can be induced to adopt a structure with functional properties very similar to those of native wild-type VDAC and that the gating properties of VDAC are thus not substantially affected by the posttranslational mod-

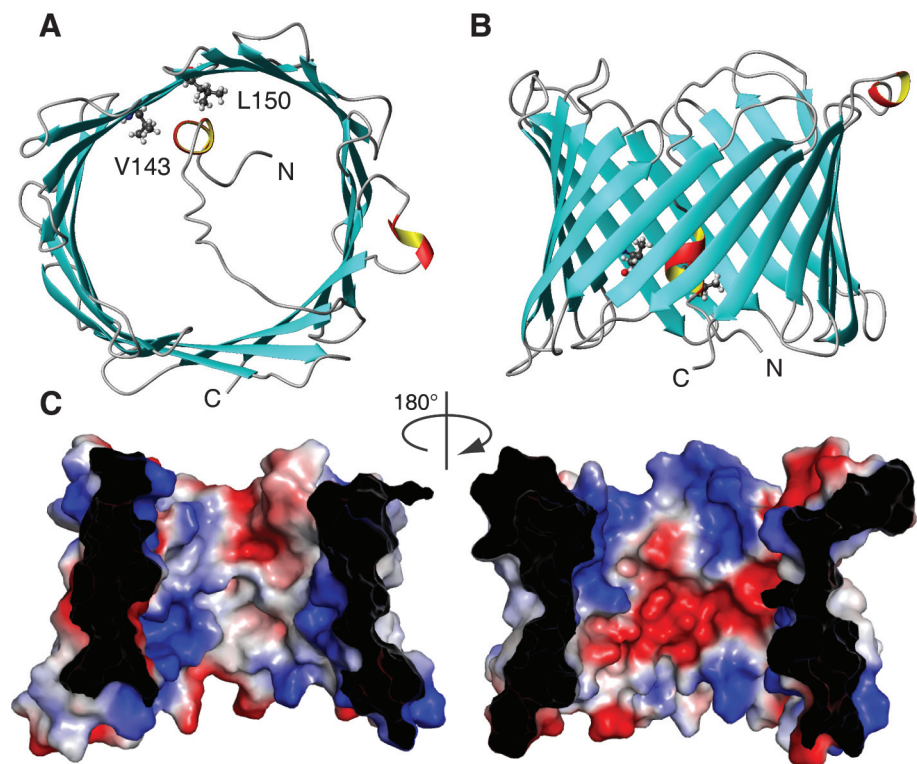


**Fig. 2.** NMR solution structure of VDAC-1 in LDAO micelles. (A and B) Top and side views, respectively, of the conformer closest to the mean of the conformational ensemble in ribbon representation.  $\beta$  sheets are shown blue, and  $\alpha$  helical secondary structures in red and yellow. N- and C-terminal and residues L150 and V143 are indicated. (C) Van der Waals surface of VDAC-1. The surface is colored according to the surface potential, calculated by using vacuum electrostatics in the program PyMOL (38). Blue indicates positive charge, and red, negative charge.

ifications in native VDAC or by the C-terminal His tag present in our preparations.

Because cholesterol was necessary to obtain wild-type-like function of recombinant VDAC-1 and because mammalian VDAC has tightly bound cholesterol (35), we used chemical shift mapping to examine the effect of cholesterol on

recombinant VDAC-1 in LDAO micelles (fig. S12). The overall structure of VDAC-1 in LDAO micelles is unchanged by cholesterol concentrations up to 1:5:400 for VDAC-1:cholesterol:LDAO. The chemical shift changes induced by cholesterol revealed two distinct interaction sites located at  $\beta$  strands 7 and 8 and  $\beta$  strand 11 (Fig. 4A).

Cholesterol is dissolved in the hydrophobic phase of the micelle and thus approaches the residues at these interaction sites from the outside of the barrel.

Weak interactions with VDAC have also been reported for some of its water-soluble natural ligands, such as adenosine triphosphate (ATP) (13). NMR chemical shift mapping indicates that neither ATP nor  $\beta$ -NAD interacts with a specific site of VDAC-1 (fig. S13). However, for the interaction with  $\beta$ -NADH, a distinct interaction surface was observed at strands 17 and 18 involving residues G242, L243, I244, A261, L263, and D264 (36) (fig. S13 and Fig. 4B). Our results are consistent with a study of native VDAC, which showed that  $\beta$ -NADH but not  $\beta$ -NAD favors the closure of VDAC and predicted that the  $\beta$ -NADH binding site would comprise the partial Walker B motif SALLD (36) at residues 260 to 264 (37).

We have mapped the binding site of the native binding partner Bcl-x<sub>L</sub> onto reconstituted VDAC-1 (Fig. 4C and fig. S14). Bcl-x<sub>L</sub> binds to VDAC-1 on strands 17 and 18. Interestingly, the loops adjacent to the Bcl-x<sub>L</sub> binding site contain several basic residues (Lys 266, 252, 200, and 201), so that this face of the molecule has a positive electrostatic surface. Bcl-x<sub>L</sub>, with an estimated pI of 4.9, is negatively charged at neutral pH, and the interaction between VDAC-1 and Bcl-x<sub>L</sub> may thus contain a substantial electrostatic component. Some residues affected by Bcl-x<sub>L</sub> binding are not located closely to this binding site. These effects could originate from allosteric changes or from a second Bcl-x<sub>L</sub> binding site at the lumen opening.

### References and Notes

1. T. Hodge, M. Colombini, *J. Membr. Biol.* **157**, 271 (1997).
2. T. Rostovtseva, M. Colombini, *Biophys. J.* **72**, 1954 (1997).
3. M. J. Sampson *et al.*, *J. Biol. Chem.* **276**, 39206 (2001).
4. K. D. Hinsch *et al.*, *J. Biol. Chem.* **279**, 15281 (2004).
5. M. G. Vander Heiden, C. B. Thompson, *Nat. Cell Biol.* **1**, E209 (1999).
6. N. Brustovetsky, J. M. Dubinsky, B. Antonsson, R. Jermerson, *J. Neurochem.* **84**, 196 (2003).
7. T. K. Rostovtseva *et al.*, *J. Biol. Chem.* **279**, 13575 (2004).
8. S. Desagher, J. C. Martinou, *Trends Cell Biol.* **10**, 369 (2000).
9. N. N. Danial, S. J. Korsmeyer, *Cell* **116**, 205 (2004).
10. G. Kroemer, L. Galluzzi, C. Brenner, *Physiol. Rev.* **87**, 99 (2007).
11. S. Shimizu, M. Narita, Y. Tsujimoto, *Nature* **399**, 483 (1999).
12. M. G. Vander Heiden *et al.*, *J. Biol. Chem.* **276**, 19414 (2001).
13. T. J. Malia, G. Wagner, *Biochemistry* **46**, 514 (2007).
14. L. Thomas, E. Blachly-Dyson, M. Colombini, M. Forte, *Proc. Natl. Acad. Sci. U.S.A.* **90**, 5446 (1993).
15. S. Stanley, J. A. Dias, D. Darcangelis, C. A. Mannella, *J. Biol. Chem.* **270**, 16694 (1995).
16. C. A. Mannella, *J. Cell Biol.* **94**, 680 (1982).
17. X. W. Guo, P. R. Smith, C. A. Mannella, *J. Struct. Biol.* **114**, 41 (1995).
18. M. Colombini, *Nature* **279**, 643 (1979).
19. M. Colombini, *Mol. Cell. Biochem.* **256**, 107 (2004).
20. D. A. Koppel *et al.*, *J. Biol. Chem.* **273**, 13794 (1998).
21. Information on materials and methods is available on Science Online.

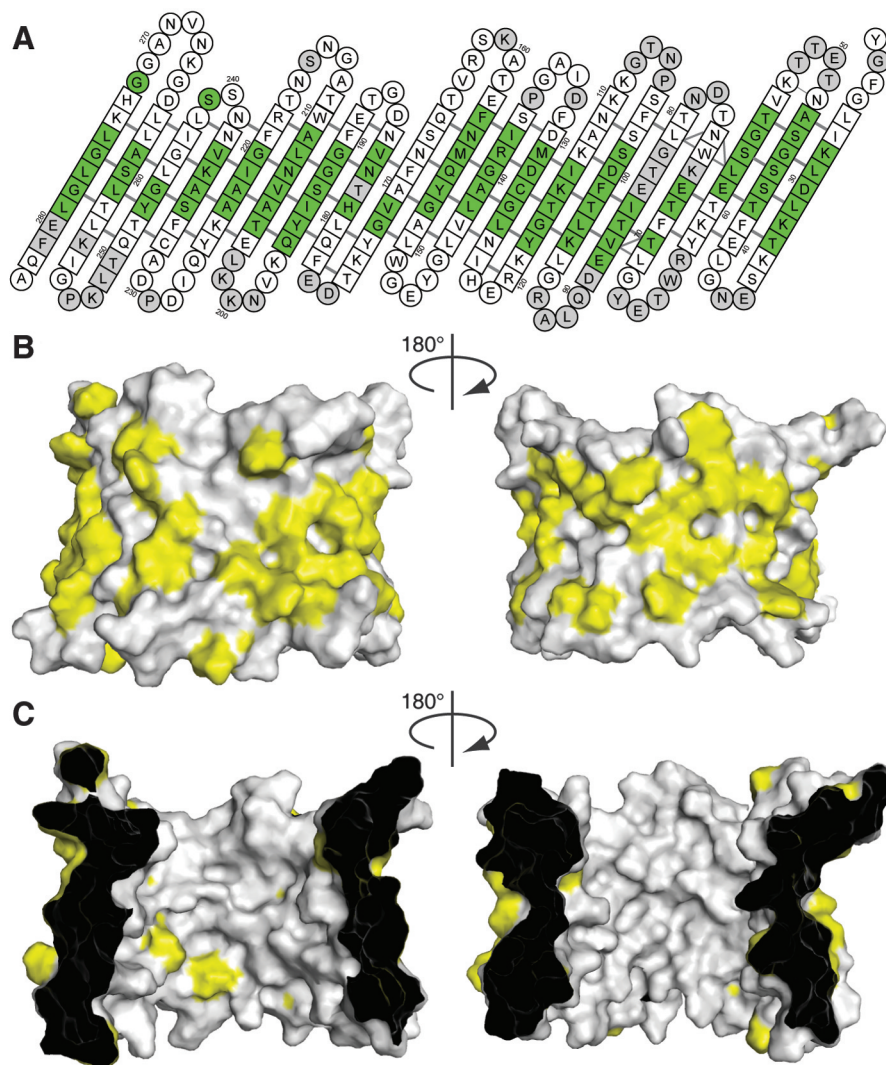


**Fig. 3.** Hydrophobic surface of VDAC-1. (A) Result of a titration with the spin-labeled detergent 16-DSA. Residues with a relaxation enhancement  $\epsilon > 20 \text{ s}^{-1} \text{ mM}^{-1}$  are green (30). These residues are in close contact to the hydrophobic interior of the micelle. Residues with  $\epsilon \leq 20 \text{ s}^{-1} \text{ mM}^{-1}$  are white. Gray residues are unassigned. Residues 1 to 21 have been omitted; no interaction with the spin label was observed for these. (B and C) Surface plot of outer and inner surfaces of VDAC-1, respectively, with the side chains of the hydrophobic residues Leu, Val, Ile, Met, Phe, and Trp shown in yellow and all other residues in white.

**Table 1.** Functional properties of VDAC voltage gating in lipid bilayers. Human VDAC-1 properties obtained from this study (see also fig. S11); rat VDAC properties are from (34).

	Recombinant human VDAC-1	VDAC isolated from rat liver mitochondria
Single conductance (nS)	$3.9 \pm 1.4$	4.0–4.5
Voltage sensor valence	2.5–4.0	3.5–4.5
$\Delta E_{\text{open/closed}}$ (kJ mole <sup>-1</sup> )	$9 \pm 2$	$10 \pm 3$
Ion selectivity $P_{\text{Cl}^-}/P_{\text{K}^+}$	1.4–1.6	1.7–1.8

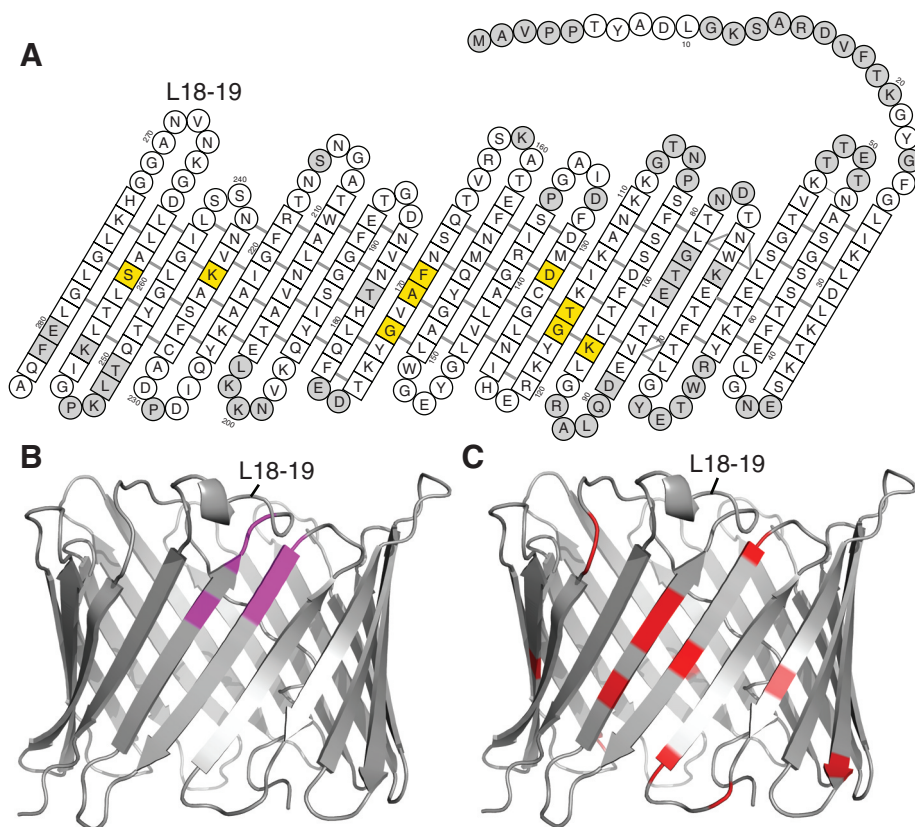


**Fig. 4.** Interactions of VDAC-1. In all three panels, the loop connecting strands 18 and 19 is indicated for orientation. **(A)** Residues with substantial chemical shift changes [ $\Delta\delta(\text{HN}) > 0.05$  ppm] caused by cholesterol binding are shown in yellow (fig. S12). The amino acids of VDAC-1 are shown as in Fig. 1A. **(B)** Amide resonances of VDAC-1 with substantial chemical shift changes (fig. S13) caused by  $\beta$ -NADH are labeled magenta in this ribbon representation; all other residues are gray. **(C)** Residues involved in Bcl- $x_L$  binding (13) are marked red in this ribbon representation; all other residues are gray.

22. M. K. Rosen *et al.*, *J. Mol. Biol.* **263**, 627 (1996).

23. K. Wüthrich, *NMR of Proteins and Nucleic Acids* (Wiley, New York, 1986).

24. S. H. White, *Membrane Proteins of Known 3D Structure*,

[http://blanco.biomol.uci.edu/Membrane\\_Proteins\\_xtal.html](http://blanco.biomol.uci.edu/Membrane_Proteins_xtal.html) (2008).

25. M. Forte, H. R. Guy, C. A. Mannella, *J. Bioenerg. Biomembr.* **19**, 341 (1987).
26. V. De Pinto *et al.*, *ChemBioChem* **8**, 744 (2007).
27. J. Song, C. Midson, E. Blachly-Dyson, M. Forte, M. Colombini, *Biophys. J.* **74**, 2926 (1998).
28. S. J. Schein, M. Colombini, A. Finkelstein, *J. Membr. Biol.* **30**, 99 (1976).
29. A. G. Komarov, B. H. Graham, W. J. Craigen, M. Colombini, *Biophys. J.* **86**, 152 (2004).
30. C. Hilty, G. Wider, C. Fernández, K. Wüthrich, *ChemBioChem* **5**, 467 (2004).
31. V. De Pinto, G. Prezioso, F. Thinnies, T. A. Link, F. Palmieri, *Biochemistry* **30**, 10191 (1991).
32. J. Song, C. Midson, E. Blachly-Dyson, M. Forte, M. Colombini, *J. Biol. Chem.* **273**, 24406 (1998).
33. J. V. Olsen *et al.*, *Cell* **127**, 635 (2006).
34. M. Colombini, *J. Membr. Biol.* **111**, 103 (1989).
35. V. De Pinto, R. Benz, F. Palmieri, *Eur. J. Biochem.* **183**, 179 (1989).
36. Single-letter abbreviations for the amino acid residues are as follows: A, Ala; C, Cys; D, Asp; E, Glu; F, Phe; G, Gly; H, His; I, Ile; K, Lys; L, Leu; M, Met; N, Asn; P, Pro; Q, Gln; R, Arg; S, Ser; T, Thr; V, Val; W, Trp; and Y, Tyr.
37. M. Zizi, M. Forte, E. Blachly-Dyson, M. Colombini, *J. Biol. Chem.* **269**, 1614 (1994).
38. PyMOL, <http://pymol.sourceforge.net>.
39. This work was supported by NIH roadmap grant GM075879. Purchase, operation, and maintenance of instruments used were supported by NIH grants GM066360, GM47467, and EB002026. S.H. was supported by the Swiss National Science Foundation. V.Y.O. was supported by the Wenner-Gren Foundation, Stockholm. Initial research on this project was supported by the Ludwig Foundation for Cancer Research. We thank V. Gelev from FBReagents.com, Cambridge, Massachusetts, for custom synthesis of the  $^2\text{H}$ -LDAO; S. Samanta for help with the electrophysiological measurements; and D. Frueh, A. Koglin, Z.-Y. J. Sun, K. Oxenoid, and S. Jenni for technical help and valuable discussions. The atomic coordinates of VDAC-1 in LDAO micelles have been deposited at the Protein Data Bank with code 2k4t.

#### Supporting Online Material

[www.sciencemag.org/cgi/content/full/321/5893/1206/DC1](http://www.sciencemag.org/cgi/content/full/321/5893/1206/DC1)

Materials and Methods

Figs. S1 to S14

Table S1

References

3 June 2008; accepted 24 July 2008

10.1126/science.1161302

## A Structural Mechanism for MscS Gating in Lipid Bilayers

Valeria Vázquez,<sup>1,2</sup> Marcos Sotomayor,<sup>3</sup> Julio Cordero-Morales,<sup>1,2</sup> Klaus Schulten,<sup>4</sup> Eduardo Perozo<sup>2\*</sup>

The mechanosensitive channel of small conductance (MscS) is a key determinant in the prokaryotic response to osmotic challenges. We determined the structural rearrangements associated with MscS activation in membranes, using functorial measurements, electron paramagnetic resonance spectroscopy, and computational analyses. MscS was trapped in its open conformation after the transbilayer pressure profile was modified through the asymmetric incorporation of lysophospholipids. The transition from the closed to the open state is accompanied by the downward tilting of the transmembrane TM1-TM2 hairpin and by the expansion, tilt, and rotation of the TM3 helices. These movements expand the permeation pathway, leading to an increase in accessibility to water around TM3. Our open MscS model is compatible with single-channel conductance measurements and supports the notion that helix tilting is associated with efficient pore widening in mechanosensitive channels.

**M**echanosensation is involved in many physiological roles, including osmotic balance, touch, and hearing (1, 2). At the molecular level, mechanosensitivity relies on

the activity of ion channels that transduce a variety of mechanical stimuli to open a conductive pore. Mechanosensitive (MS) channels are grouped by function rather than sequence sim-

ilarity (3, 4). In prokaryotic systems, MS channels respond directly to bilayer deformations, with a transduction mechanism defined at the protein/lipid interface (5, 6). Although this is also true for some eukaryotic MS channels (7), many also respond to mechanical deformations through their association with the cytoskeletal network (8).

Although the molecular identification of eukaryotic MS channels remains challenging (2, 9, 10), the biophysical and structural properties of prokaryotic MS channels have proved far more tractable at the molecular level. The crystal structures for the MS channels of large (MscL) and small (MscS) conductance (11–13) have provided a molecular framework to interpret functional and biophysical data and have helped establish the basic mechanistic principles by which these two distinct channels sense the physical state of the bilayer (14–17). Nevertheless, given the critical role that lipid-protein interactions play in prokaryotic function (15), two questions arise: First, what is the correspondence between these crystal structures and mech-